Macrophage Phenotyping Using Autofluorescence Microscopy and Machine Learning

by

Alec Xu

B.A.Sc., The University of British Columbia, 2019

A THESIS SUBMITTED IN PARTIAL FULFILLMENT OF

THE REQUIREMENTS FOR THE DEGREE OF

MASTER OF APPLIED SCIENCE

in

THE FACULTY OF GRADUATE AND POSTDOCTORAL STUDIES

(Mechanical Engineering)

THE UNIVERSITY OF BRITISH COLUMBIA

(Vancouver)

September 2022

The following individuals certify that they have read, and recommend to the Faculty of Graduate and Postdoctoral Studies for acceptance, a thesis entitled:

Macrophage Phenotyping Using Autofluorescence Microscopy and Machine Learning

submitted by Alec Xu in partial fulfillment of the requirements for

the degree of Master of Applied Science

in Mechanical Engineering

Examining Committee:

Hongshen Ma, Associate Professor, Mechanical Engineering, University of British Columbia
Supervisor

Mu Chiao, Professor, Mechanical Engineering, University of British Columbia
Supervisory Committee Member

Mauricio Ponga, Assistant Professor, Mechanical Engineering, University of British Columbia
Supervisory Committee Member

Abstract

Macrophages are highly plastic immune cells which morph into different phenotypes depending on their surrounding environment. The two main paradigms for macrophage phenotyping are phenotyping by function and by origin. Phenotyping based on function separates macrophages into three polarizations: naïve (M0), pro-inflammatory (M1), and anti-inflammatory (M2). Phenotyping based on origin distinguishes macrophages from their place of origin. This can be from monocytes created in the bone marrow, or local proliferation from tissue resident macrophage populations. These phenotypes have different functions and can be associated with different metabolic states, which can be detected via immunofluorescence assays or autofluorescence. Detecting these phenotypes can be a powerful tool in the diagnosis of different diseases, as many diseases impact macrophage populations in the affected tissue. Currently macrophage phenotyping is difficult and requires use of unreliable surface markers or expensive sequencing techniques. In this thesis we use fluorescent microscopy-based images for the training and validation of different image-based algorithms for effective classification. We first imaged THP-1 derived M0/M1/M2 macrophages for brightfield and fluorescently stained mitochondrial images. We then applied this dataset to multiple state-of-the-art deep learning models, achieving 5-fold validation accuracy of 80.50% using PNASNet-5. We also explore phenotyping murine tissue resident macrophages, bone-marrow monocyte-derived macrophages, and monocytes. This was conducted by imaging for autofluorescence and applying to an original convolutional neural network (MacNet) as well as using CellProfiler feature engineering and classical classifiers. We achieve 97.72% validation accuracy using MacNet and 98.58% validation accuracy on CellProfiler features in random forest.

Lay Summary

Macrophages are a type of white blood cell found in most tissues in the body. They play important roles in removing pathogens and dead cells, as well as sending signals to other immune cells. Macrophages can take on different roles depending on their local environment. Knowing the role of macrophages is often helpful for diagnosing and studying different diseases. This thesis studies several ways to determine the role macrophages from microscope images using artificial intelligence.

Preface

This dissertation is original and unpublished work by the author, A. Xu. It is a continuation of the work done in Berryman et al. (2020). All of the work presented was conducted in the Multi-scale Design Lab at the University of British Columbia. All animal experiments were conducted in accordance with the Canadian Council of Animal Care Guidelines using protocols approved by the University of British Columbia Animal Care Committee. The protocol number for the experiment in chapter 3 is A19-0243.

The experimental designs in chapter 2.1 and 3.1 were primarily designed and conducted by K. Matthews. The cells used to conduct the experiment in chapter 3.1 were supplied by the Johnson Lab at UBC and cultured by Y. Huang and K. Matthews.

The design and implementation of MacNet used in chapters 2 and 3 and the CellProfiler workflow used in chapter 3 is of my own design. The other neural net architectures in chapter 3 used implementations by R. Wightman on open-source designs from various sources. All data processing, machine learning model training, testing, and interpretation were conducted by me.

Table of Contents

List of Tables

List of Figures

.

List of Abbreviations

CD	Cluster of differentiation
CNN	Convolutional Neural Network
FAD	Flavin adenine dinucleotide
GSC	Glioma stem cells
MD	Monocyte-derived
MPS	Mononuclear phagocyte system
MSC	Mesenchymal stem cell
Mtb	Mycobacterium tuberculosis
NADH	Nicotinamide adenine dinucleotide
NADPH	Nicotinamide adenine dinucleotide phosphate
TR	Tissue resident

Acknowledgements

I offer my gratitude to the staff and my fellow lab members at UBC, whose intelligence, inquisitiveness, and kindness inspire me every day.

I owe particular thanks to lab manager Dr. K. Matthews who offered me unending support for all things related to biology, and fellow lab mate Sam for always being available to give advice on research, or just to relax and unwind.

Special thanks are owed to my friends and family, whose support allowed me to continue forging ahead.

Finally, I'd like to thank my supervisor, Dr. H. Ma, for initiating me into academia, and providing unending support for both my questions in research and careers.

Dedication

To my mom, who supported me every step of the way.

Chapter 1: Introduction

1.1 Macrophages

Since the discovery of macrophages, they have played a strong role in our understanding of tissue homeostasis and inflammation. Macrophages are innate immune cells that phagocytose debris, pathogens, and dead cells. They are found in every type of tissue and are incredibly important in maintaining tissue homeostasis. Macrophages are also incredibly plastic cells and can be found in a variety of phenotypes, which they can differentiate into given specific environmental factors.

1.1.1 Macrophage Polarization as a Diagnostic Tool

One axiom of macrophage phenotypes is their polarization. The polarization of a macrophage describes its function in tissue. A macrophage can acquire an M0 (unpolarized), M1 (classical), or M2 (alternative) phenotype. M1 macrophages are typically associated with an inflammatory local environment, which means they express inflammatory cytokines, activate immune cells, and generate anti-microbial NO_2 [1]. M2 macrophages are associated with homeostasis and have anti-inflammatory properties, which refers to clearing debris/dead cells and assist tissue repair by producing arginase. Currently, the most popular method of evaluating their polarization is to measure the expression of different types of clusters of differentiation (CD), chief among them CD80 or CD206[2]–[5] on the surface of the cell membrane. Some studies also use the up-regulation Arg1 and Egr2 which is measured using gene expression profiling[6].

While current literature has questioned the validity of using macrophage polarization to describe the gamut of macrophage phenotypes[1], [7], [8], it is still a useful model which can assist in

disease pathogenesis. Russel et al. observed that Mtb, the pathogen causing tuberculosis, induces an environment rich in IFN-g locally [9], which is known to induce M1 differentiation. Xu et al. reported that the fungi A. *fumigatus conidia* induced NADPH oxidation in alveolar macrophages, suggesting an M1 phenotype [4]. Bhatia et al. also found that *Aspergillus fumigatus* infection caused alveolar macrophages to express key markers associated with M2 macrophages [5]. By correctly identifying macrophage phenotypes in the disease environment, we can greatly narrow down the range of possible diseases.

1.1.2 The Origins of Macrophages

Macrophages were originally believed to be solely derived from circulating monocytes via the mononuclear phagocyte system (MPS) model [10], this belief has since been discarded. We now know that macrophages populate our tissues in 3 waves; the first wave from primitive yolk-sac macrophages, the second from the fetal liver, and finally monocytes derived from hematopoietic precursors in the bone marrow[11]–[13]. The first two waves form stable populations in tissue and are known as “tissue resident” (TR) macrophages, while the latter wave replenishes macrophages in tissue, and are known as “monocyte-derived” (MD) macrophages.

Most TR macrophage populations are self-sustaining but are supplementally replenished from monocytes gradually throughout life[13], or rapidly during infection/inflammation[14]. Recently, it has been shown that the presence of MD macrophages can signify disease or abnormal conditions[14]–[16], and that MD macrophages can acquire a TR phenotype, indistinguishable transcriptionally and functionally[14] after homeostasis is re-established.

1.1.3 TR vs MD Macrophages Phenotypes as a Diagnostic Tool

Another axiom of macrophage phenotyping is their origin. The origin of the macrophage is of interest due to evidence of its use as a diagnostic tool. Aegerter et al. showed that Influenza infection rapidly deplete TR macrophages, and cause elevated levels of MD phenotype for months after infection, after which they assume a TR phenotype [14]. Lai et al. also observed that there is a depletion of TR phenotype during malaria infection, which was recovered 14 days after infection in the lung[17]. In general, infections seem to deplete TR macrophages to different degrees, and the speed in which the TR phenotype replenishes vary with different illnesses.

Novel micro-targeted therapy techniques can also benefit from accurate identification of macrophage phenotypes. Pierre et al. showed that interstitial TR macrophages were associated with oncological tumor growth in murine models, while MD macrophages were associated with tumor spreading, then clearance after chemotherapy[18].

1.2 Current State of Macrophage Phenotyping

Currently macrophage polarization analysis suffers from subjectively gating values for surface stains and destructive staining for intracellular stains and RNA. There are often no clear divides between macrophage polarization measurements. Rather than act as discrete categorizations, these phenotypes behave more as polar extremes of a spectrum.

Figure 1. shows that Liu et al. used surface marker expression to classify macrophage polarization [19]. Gates were chosen to divide a continuous distribution of cells. This technique

is currently one of the most common in the field of macrophage phenotypes. Other surface markers include CD301 [20] for M2 polarization and CD38 [6] for M1 polarization.

Another method to determine macrophage polarization is to evaluate regulation of specific genes within the cell such as Arg1, NOS2 or EGR2 [5], [6], [20]. This can be achieved by either using intracellular stains for the specific enzymes produced, or by conducting PCR on RNA to determine the level of expression of each gene. In either case the cell does not survive analysis, and these methods are more involved than the other methods currently in use.

Compared to macrophage polarization phenotyping, we can also phenotype macrophages by their origin. This is more difficult to execute due to the incredible plasticity of macrophages, allowing even cells of different origin to converge toward indistinguishable phenotypes.

Fate-mapping involves altering cells in the murine-embryo with a tagging protein. This precludes its use in fully-grown specimen, as well as humans, limiting usefulness. The parabiosis approach surgically joins two specimen and monitors the level of chimerism in tissues and blood after certain time periods. Hashimoto et al. utilized fate-mapping and parabiosis to conclusively show the diverse origin of macrophages [21]. Zhu et al. also used parabiosis to demonstrate monocyte-based replenishment of macrophages in tumors [3]. This method is even more restrictive than fate-mapping and would be impossible to transfer to humans as well.

It is also possible to phenotype macrophage by origin using expression of associated proteins. Similar to phenotyping polarization, Aegerter et al. identify upregulated genes using ATAC-seq

such as CCR2 associated with MD macrophages [14]. Lai et al. used conventional flow-cytometry techniques to associate F4/80 to tissue-resident macrophages and CD11b to MD macrophages [17]. These methods have the same drawbacks as when applied to macrophage polarization.

1.3 Fluorescence and Autofluorescence Imaging

Fluorescence imaging refers to capturing the glow of fluorescent dyes or proteins which correspond to different parts of the cell [22]. Conventionally in immunofluorescence, antibodies bind with specific targets in the cell. These antibodies either have attached fluorophores themselves, or act as magnets to other antibodies with attached fluorophores. After staining is complete, the excess fluorescent antibodies are washed away. The sample is then excited using lasers of a specific wavelength, allowing it to fluoresce. A major issue with immunofluorescence is non-specific binding, where the antibody binds to parts of the cell other than its target. Non-specific binding, photobleaching [23], [24] (the attenuation of fluorescent signal while excited), and inconsistent dye preparation causes difficulty in capturing high-quality and consistent fluorescent images.

Autofluorescence imaging is another method of fluorescence imaging that conveniently avoids issues such as photobleaching and inconsistent dye preparation of immunofluorescence. Autofluorescence imaging is conducted by exciting fluorophores that naturally exist in the cell, bypassing the need to apply fluorescent antibodies for certain applications. In recent years, there has been a focus on the naturally fluorescent metabolic enzymes NADH, NADPH, and FAD. These enzymes are found throughout the cell and particularly in lipogenesis [25], which could

mean that autofluorescence imaging highlights lipid droplets. Autofluorescence imaging has in particular been used to classify immune cells. Using fluorescence lifetime imaging (FLIM), Walsh et al. recorded the autofluorescence of cells through time, then fed the resulting image into a random forest algorithm to predict quiescent and activated states [26].

1.4 Mitochondria Imaging as a Phenotyping Tool

Mitochondria are organelles in the cell responsible for generating energy in the form of ATP for cellular functions. They do this via two major metabolic pathways; glycolysis and oxidative phosphorylation (OXPHOS). While glycolysis provides an abundance of immediate energy, it is less efficient than OXPHOS [27]. These pathways are closely linked to the metabolic state of the cell. In macrophages, mitochondria are found to be fragmented in a pro-inflammatory M1 state, mainly generating ATP through glycolysis. Conversely, they fuse together into elongated shapes and primarily generate ATP via OXPHOS in the anti-inflammatory M2 state [28], [29].

Mitochondria can be detected using targeted stains, or via autofluorescence. This is due to the fluorescent enzyme NADH, which predominantly exists in its bound form in mitochondria [29]. This is also related to lipolysis, as lipids are one of the metabolic fuels that mitochondria use to produce ATP [30]. We can establish a link between mitochondria, lipids, and autofluorescence and their differing states between macrophage phenotypes.

1.5 Computer Algorithms for the Categorization of Cellular Microscopy Images

Current cell measurement techniques such as flow cytometry or fluorescence intensity gating leave a lot of information unharvested from biological samples. Each sample is reduced to a few measurements. By gathering data-rich microscopy images and incorporating computer algorithms into their analysis, we can obtain all the previously gathered information and much more.

A typical workflow incorporating computer algorithms will include data gathering, post-processing/feature extraction, and finally categorization. Initially, imaging techniques such as Raman spectroscopy, immunostaining microscopy, or FLIM are used to gather raw image data. The resulting image data can optionally be processed using software like CellProfiler or Fiji to run algorithms such as watershed segmentation, color LUT adjustments, or texture/granularity measurements. Often, these measurements themselves yield sufficient insight into a topic of interest. If the goal is categorization of cells, these measurements can then be fed into a plethora of categorizers such as random forest or K-Nearest-Neighbors. The raw image can also be used as-is and fed into convolutional neural networks or other deep-learning-based methods. These methods rely on showing a network of connected nodes many images to tune a set of parameters until the network classifies images correctly.

Recently, the use of computer algorithms has become more common in macrophage phenotyping. Rostam et al. previously demonstrated that preprocessing images of stained macrophages using CellProfiler coupled with classical techniques can achieve high classification accuracy for macrophage phenotypes [2]. Pavillon et al. used autofluorescence and Raman

spectroscopy combined with logistic regression models to attain high classification accuracies on macrophage phenotypes [31]. As mentioned before, Walsh et al. used autofluorescence and basic classifiers such as random forest to classify T-cells to very high accuracy [26].

We can also look at the phenotyping of other cells for techniques that may apply to macrophage phenotyping as well. Toth et al. found that by extracting features from the surrounding environment of microscope-imaged cells using CellProfiler, they could obtain high accuracies classifying both the MCF-7 cell line as well as cancerous urinary bladder tissue [32]. Berryman et al. showed that a small convolutional neural network (CNN) could accurately identify different cancer cell lines using brightfield and fluorescent channels [33]. Single channels of fluorescence allowed for relatively high accuracies, but brightfield did not. Finally, we recently see advances in using machine learning in the prediction of fluorescent labels from non-fluorescent images such as brightfield [34], [35]. This involves "coloring" in a brightfield image with regions of interests such as DNA, mitochondria, and various other parts of the cell without using fluorescent dyes. Using predictive regions of interest with feature extraction could enable interpretable classification with many of the benefits of machine learning.

1.6 Research Goals and Contribution

The rapid and accurate classification of macrophage phenotypes has the potential to unlock a whole new class of diagnostic and treatment tools, but is hindered by the difficulty, cost, and reliability of current methods. While using brightfield as the only imaging channel for identification is fast and easy, it has given subpar performance on actual classification. Specific

stains impart high accuracies but are time-consuming and can be inconsistent. Imaging autofluorescence is one way to increase performance while not requiring excessive effort or time.

In this thesis we show that using brightfield and autofluorescence images, high classification accuracies can be attained with small image sets in classifying macrophage phenotypes by origin. we also show that using brightfield and mitochondrial stains, relatively high classification accuracies can be achieved when phenotyping macrophage polarization. This is demonstrated by training and validating different CNN and image-based deep learning networks to classify macrophage polarization and origin.

The main novelty in this thesis is our use of autofluorescent snapshot images of macrophages for the classification of their phenotype. While others have classified macrophages using fluorescence lifetime microscopy, classifying via autofluorescence images without a temporal element is still novel. We also notice a lack of using machine learning for classification of macrophage phenotypes, with many papers preferring to pair their preferred imaging modality with older classification methods such as linear regression or random forest.

Chapter 2: Classifying Macrophage M0/M1/M2 Phenotypes

2.1 Experimental Design for M0/M1/M2 Macrophage Phenotypes

2.1.1 Cell culture and differentiation

The human leukemia monocytic cell line, THP-1 (ATCC TIB-202) cells were used in this study. THP-1 cells were cultured in Roswell Park Memorial Institute medium (RPMI 1640, Invitrogen) containing 10% v/v Hi-FBS (Invitrogen) and 0.05 mM ß-mercaptoethanol (Sigma-Aldrich). THP-1 monocytes were differentiated into M0 macrophages by 24 h incubation with 150 ng/ml phorbol 12-myristate 13-acetate (PMA, Sigma, P8139) followed by 24 h incubation in complete RPMI medium based on a published protocol [1]. After this, M1 macrophage polarization was obtained by incubation with 20 ng/ml of interferon gamma (IFN-γ, R&D system) and 10 pg/ml of lipopolysaccharide (LPS, Sigma-Aldrich) for a further 24 h. M2 polarization was achieved by incubation with 20 ng/ml of interleukin 4 (IL4, R&D Systems) and 20 ng/ml of interleukin 13 (IL13, R&D Systems) for 72 h. All cells were maintained at 37 °C in an incubator supplied with 5% CO2 and grown to 70-90% confluency before experiments.

2.1.2 Immunostaining

M0, M1 and M2 differentiated cells were detached from culture flasks using StemPro Accutase solution (Gibco, Invitrogen), followed by gentle scraping. All M0, M1 and M2 cells were stained with mouse anti-human CD80 – BV421 (Clone L307.4, 564160, BD Biosciences) and rabbit anti-mannose (CD206) receptor-Alexa Fluor 647 ([EPR6828(B)], Ab195192, Abcam) for immunophenotyping following the manufacturer's instructions. All cells were also stained with 75nM MitoTracker Green FM (M7514, Invitrogen). The cells were then washed twice with phosphate buffered saline (PBS, Invitrogen) with 0.1% Bovine Serum Albumin (BSA,

Invitrogen) to remove unbound proteins. Finally, the cells were plated in RPMI (no phenol red, Invitrogen) supplemented with 10% HI-FBS in 96-well glass-bottomed imaging plates (Greiner Sensoplate, Millipore Sigma).

2.1.3 Microscopy

Microscopy imaging was performed using a Nikon Ti-2E inverted fluorescence microscope. Images were acquired using a Nikon CFI Plain Fluor 20X objective and a 14-bit Nikon DS-Qi2 CMOS camera. Images were captured using 4 channels: brightfield with phase contrast, DAPI (Nikon C-FLL LFOV, 392/23nm excitation, 447/60nm emission and 409nm dichroic mirror), Cy5 (Nikon C-FLL LFOV, 562/40nm excitation, 641/75nm emission and 593 dichroic mirror) and EGFP (Nikon C-FLL LFOV, 466/40nm excitation, 525/50nm emission and 495nm dichroic mirror). Illumination for brightfield imaging was performed using the built in Ti-2E LED. Describe SOLA. Gain, exposure and vertical offset were automatically determined using built-in NIS functions to avoid user biasing. Cells were imaged in Greiner Sensoplate 96-well glass bottom multiwell plates (M4187-16EA, Sigma-Aldrich). The concentration of cells in each well were diluted down to approximately 1000 cells to ensure adequate spacing between adjacent cells. An automated procedure was run on NIS using the Jobs function to take 36 images, on each of the 4 channels, inside of each well. The images were exported from NIS to standard TIFF format.

2.2 Data Processing for M0/M1/M2 Macrophage Phenotypes

2.2.1 Sample selection and augmentation

Custom software written in Python was used for manual framing of desired samples in bounding boxes of size 96 by 96 pixels. Samples were chosen based on isolation and clarity. Apoptotic cells and debris were discarded. 3000 samples each of M0, M1, and M2 macrophage phenotypes were labeled. The dataset was further enhanced for CNN training by applying 90-degree rotations to the image randomly before using the samples for training.

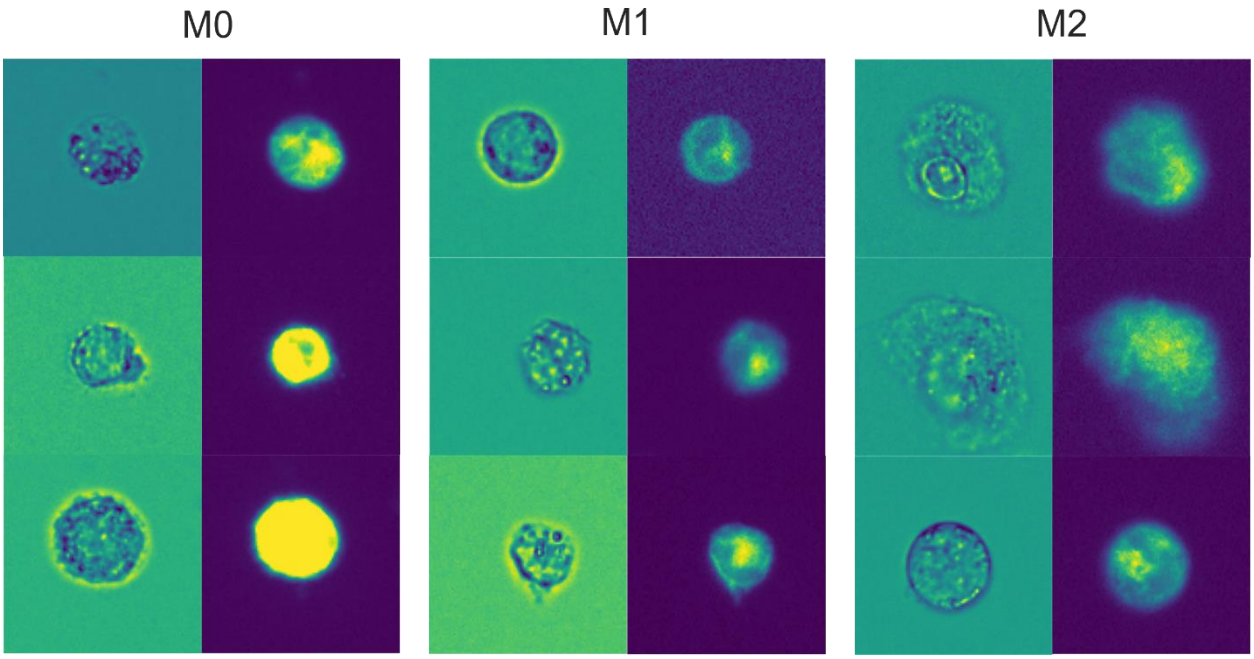

Figure 1. Sample's of M0, M1, and M2 macrophages segmented manually. On the left is the brightfield channel while on the right is the mitochondrial stain shown in the EGFP channel.

2.2.2 Training environment

The model was trained on an Alienware m15 R4 with 16GB of RAM, Intel® Core™ i7-10870H CPU, and NVIDIA GeForce RTX 3070 GPU with 8GB of VRAM. We used Anaconda for dependency management, with core libraries including Python 3.7.10, Pytorch 1.8.1, pandas 1.2.2, numpy 1.19.2 and timm 0.5.5.

2.2.3 CNN Model: MacNet

MacNet is a convolutional neural network of 2.5million parameters implemented in Pytorch. The default input into the model is a 96x96 pixel single-channel image. A series of 3x3 convolutional layers is used to extract features from the input, with no padding as to de-emphasize features on the edge of the image. 2-by-2 maxpools are performed every other filter layer to reduce overfitting and boost generalizability. The output of the convolutional layers is fed into 3 256 wide dense layers with 20% dropout to prevent overfitting. The dense layers feed into an 3-wide output, corresponding to number of possible classes. The node with the highest activation is the predicted output of MacNet.

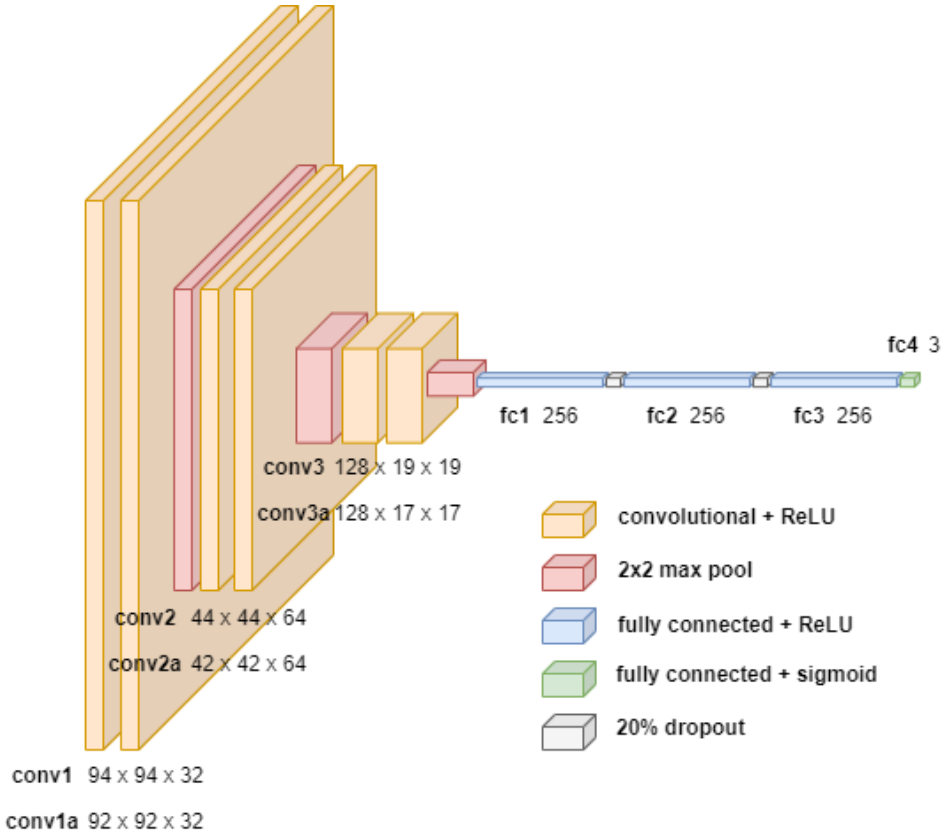

Figure 2. MacNet Architecture.

2.2.4 Training MacNet CNN

MacNet was trained using 2 channels of 96x96 pixel input. The two input channels were brightfield, and mitochondrial stains of differentiated macrophages. Random 90 degree were used to augment the dataset. The dataset consisted of 3000 samples for each class, for a total of 9000 images. These were stored as binaries - Python Serialized Object (pickle) - and loaded into the custom training script. The dataset was then split into 5 folds for 5-fold cross-validation using the Adam optimizer.

2.2.5 Training and Comparing to State-of-the-art Image Classification Architectures

Due to the inadequate performance of MacNet on macrophage polarization classification, we evaluated the performance of other state-of-the-art networks as well. These networks are:

1. EfficientNet B0: A CNN which aims for high efficiency. B0 is the smallest variant [36].
2. EfficientNet B2: A CNN which aims for high efficiency. B2 is the 3rd smallest variant [36].
3. Inception v4: A fully convolutional neural net known for excellent performance [37].
4. PNASNet-5: A model found by the progressive neural architecture search algorithm [38].
5. ResNext: An residual network using high cardinality equivalent residual blocks[39].

We trained these networks using the Pytorch Imaging Models (timm) library [40]. This library provides implementations for each model, as well as supporting training and inference scripts. These scripts were modified to work with our data and workflow.

2.3 Results for Classification of M0/M1/M2 Macrophage Phenotypes

2.3.1 Classification Results

The highest accuracy achieved was 80.50% by PNASNet-5, as evaluated by 5-fold cross validation. This accuracy is not particularly high, but entirely within the expected range. Due to the difficulty in achieving perfect differentiation of macrophages, some of cells in each cohort may not belong to its label. This seems to be supported by the confusion matrix and T-SNE, where M0 samples are quite well categorized but M1 and M2 samples seem mixed. Pavillon et al. noticed similar problems when using batches of macrophage subjected to different activation treatment as labels [31].

Architecture	Params	Accuracy
PNASNet-5	86M	80.50%
Inception_v4	43M	79.32%
Efficientnet_b2	9M	77.48%
ResNeXt	89M	77.24%
Efficientnet_b0	5M	77.08%
MacNet	2.5M	72.22%

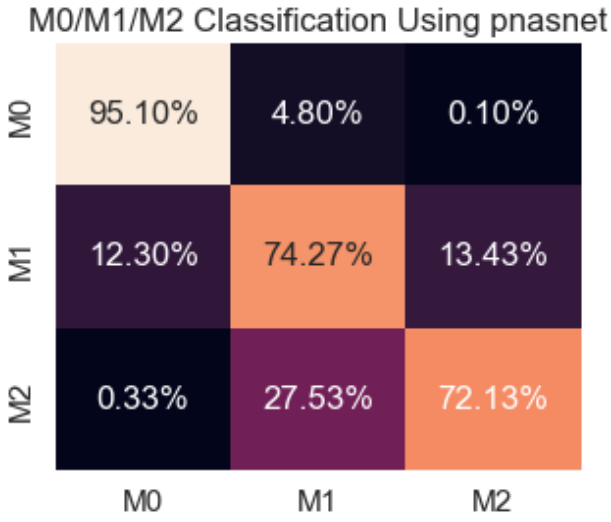

Figure 3. left) Architecture size and accuracy for classifying macrophages based on function. Right) Confusion matrix of highest performing PNASNet classifier.

The comparison between different architectures is also quite interesting. Inception v4 managed to achieve very similar performance with PNASNet-5 with half the number of parameters. MacNet was the worst performing, but also the smallest model by far. ResNeXt, while the largest model, performed similarly to Efficientnet B2, which is around $1/10^{th}$ of its size. We can see that both model size and architecture are very important.

2.3.2 Evaluating Model Effectiveness

Below is the T-SNE plot of the final layer of PNASNet-5 before output. Homogenous, clearly separated groups is ideally what we would see for accurate and non-overfit classification. What we see here is a continuous band, with frequent mixing between classes. Band-like patterns can appear in T-SNE plots when the samples collected are not time-invariant. This suggests that some level of fluorescence intensity change occurred when imaging; most likely photobleaching of the mitochondrial stain. The lack of distinct groups also further suggests that at least using this current phenotyping paradigm, the phenotypes are more of a spectrum than discrete classes.

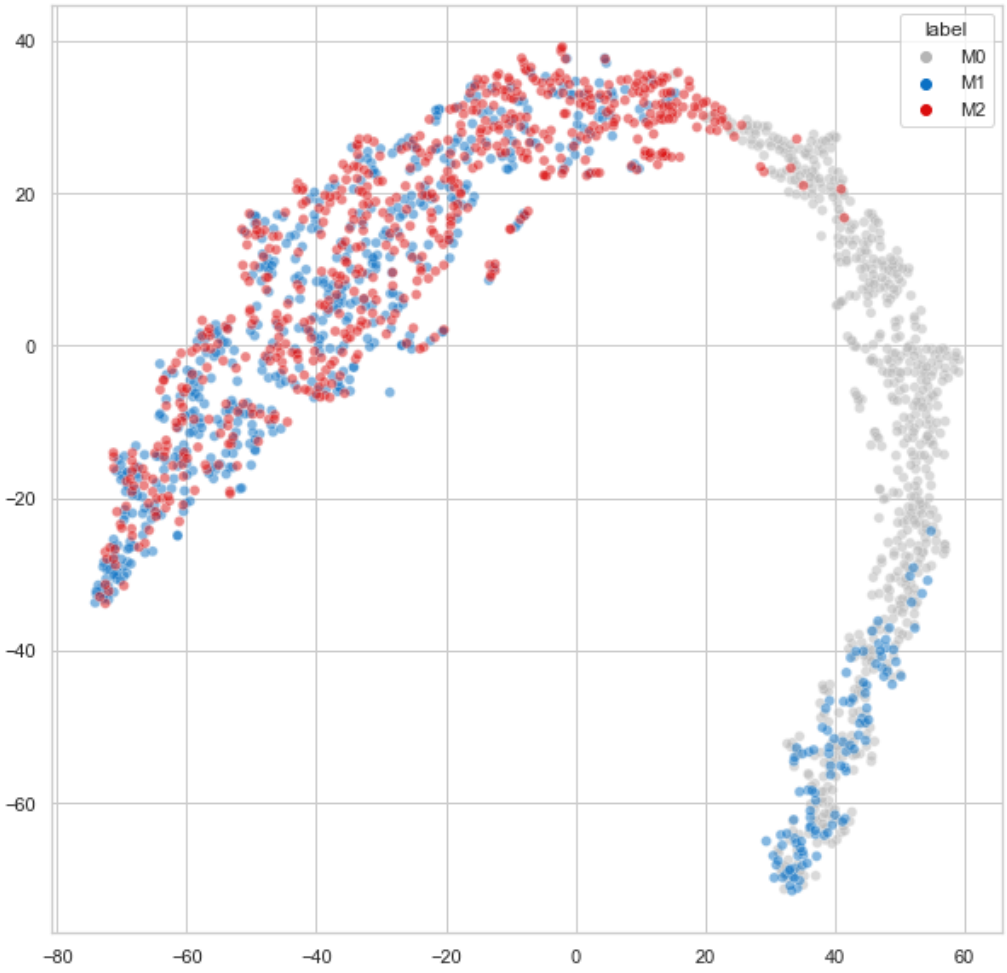

Figure 4. T-SNE describing final layer of PNASNet-5 before classification. The clustering suggests that while M0 differentiation is quite successful, M1 and M2 differentiations are incomplete.

We also used the DEEPLift saliency map algorithm to generate pixel attribution maps based on input. From what is shown below, we see most of the activated pixels are within the cell, and roughly correlate to features inside the cell. This suggests that the model is actually classifying off the morphology of the cell rather than imperfections in the background (different light levels, debris).

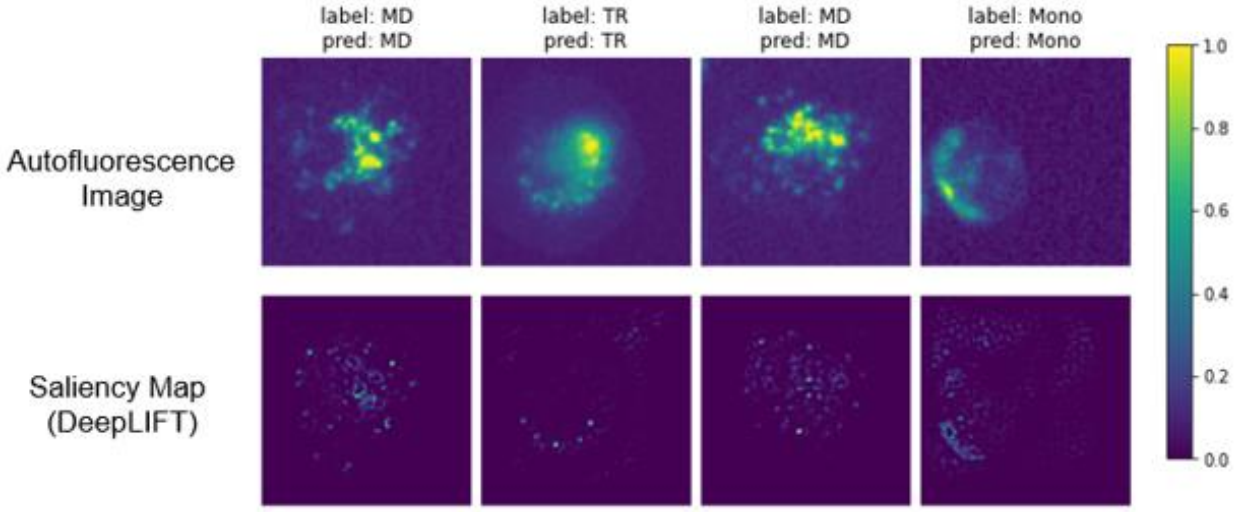

Figure 5. The autofluorescence input is shown above while DEEPLift saliency map for pixel activation is show below. Most bright saliency map pixels are inside the cell, suggesting the classifier is using actual features in the cell

2.4 Discussion

From our results, we can see that it is possible to distinguish macrophage polarization to a moderate degree of accuracy. We see one roadblock in increasing this accuracy further is due to the current state-of-the-art method for labeling, which relies on surface markers. These surface markers present macrophage phenotypes as more of a spectrum rather than discrete classes. Some success has been shown by identifying macrophage populations by gene expression [6], but accuracy on the single cell level is required for a robust testing and training dataset.

A possible improvement to categorizing macrophage polarization is to try and predict surface marker expression instead of phenotype. To do this we could use surface marker stain intensity as the label instead of the phenotype. This would conveniently bypass the need for cohorts to be pure and would be a more objective measurement. One challenge would be the calibration of fluorescence intensity in different batches of images. Currently, we can apply normalization and standardization freely as we do not measure quantitative information. This would change if we tried to use the fluorescent intensity as the label. This problem can be addressed using fluorescence reference beads, and calibrating results using these references.

We can also ask the question of whether the macrophage activation paradigm really sufficiently describes macrophage phenotypes. Current research has been moving either towards an ever-expanding array of macrophage activation states, or another phenotyping paradigm altogether. Macrophage activation can be subjective by using different gates, secretions, and biomarkers. The origin of the macrophage is less subjective and could perhaps be the key to phenotyping macrophages and their overlapping functionality.

Chapter 3: Classifying Macrophage Origin Phenotypes

3.1 Experimental Design for TR Macrophages/MD Macrophages/Monocytes

Three cohorts of cells were collected from mice. Monocytes from the blood, alveolar (TR) macrophages from the lung, and MD macrophages derived from bone-marrow monocytes. These cohorts were pelletized, washed, and plated separately into a 384 well plate (Greiner Sensoplate, M4187) for imaging.

3.1.1 Animals

C57BL/6 J mice were bred and housed at the University of British Columbia. All animal experiments were conducted in accordance with the Canadian Council of Animal Care Guidelines using protocols approved by the University of British Columbia Animal Care Committee (A19-0243).

3.1.2 MD Macrophages from Femur

Bone marrow cells were isolated from the femurs of mice and treated with RBC lysis buffer. Subsequently, 1.5 × 107 cells were cultured in 10 ml of DMEM, 20% FBS, 1 mM sodium pyruvate, 2 mM L-glutamine, 50 U/ml penicillin/streptomycin, and 8% L929 cell-conditioned media as a source of CSF-1. Bone-marrow monocyte-derived macrophages were harvested using Versene at day 5 for further analysis.

3.1.3 Alveolar macrophages harvested from bronchoalveolar lavage

Alveolar macrophages were harvested by bronchoalveolar lavage via catheterization of the trachea and washing three times with 1 ml 1× PBS, 2% BSA, and 2 mM EDTA. Subsequently, cells were pelleted and treated with RBC lysis buffer prior to analysis.

3.1.4 Image acquisition

Samples were imaged overnight on a Nikon Eclipse Ti2-E inverted microscope by exciting with a 500nm light source and detecting 525nm emissions. For each set of images, exposure was set to 1 second. Gain was set to 31.4x for alveolar macrophages and MD macrophages, and 38.4x for monocytes.

3.2 Data Processing for TR Macrophages/MD Macrophages/Monocyte Phenotypes

3.2.1 Sample selection and augmentation

Custom software written in Python was used for manual framing of desired samples in bounding boxes of size 96 by 96 pixels. Samples were chosen based on isolation, clarity, and illumination. Apoptotic and irregular cells were discarded. After final selection, 2329 alveolar macrophages, 2000 MD macrophages, and 2000 monocytes were found. The dataset was further enhanced for CNN training by applying 90-degree rotations to the image randomly before using the samples for training.

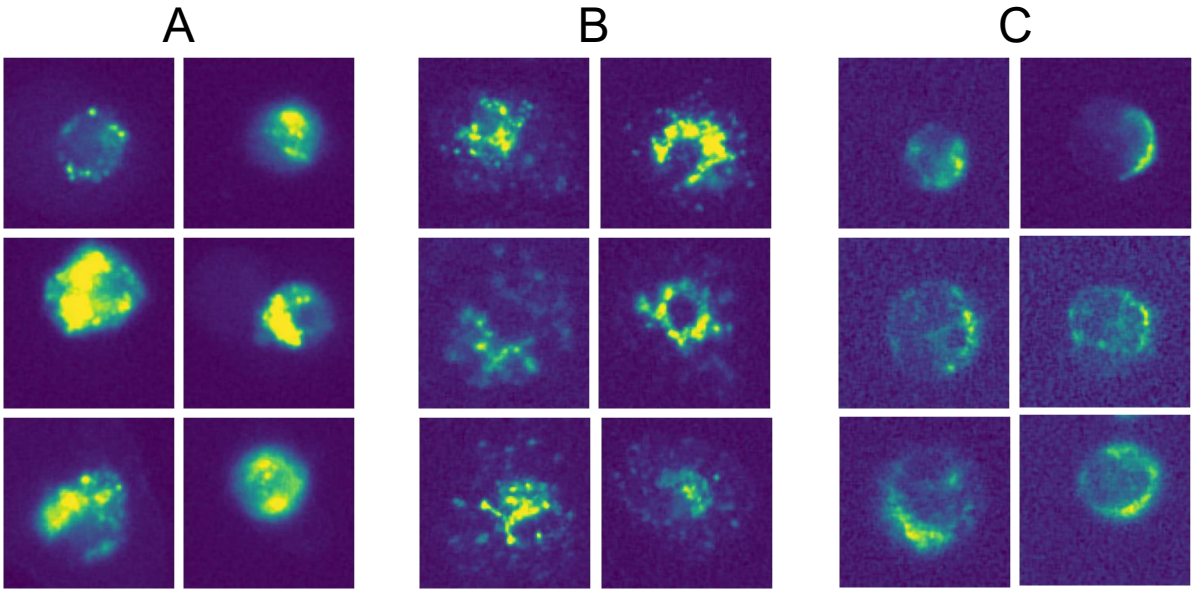

Figure 6. Autofluorescent samples from A) TR Macrophages, B) MD Macrophages, and C) monocytes. Samples are 96x96 px in shape and were segmented from large TIFF images captured by the microscope.

3.2.2 Training environment - MacNet

The model was trained on an Alienware m15 R4 with 16GB of RAM, Intel® Core™ i7-10870H CPU, and NVIDIA GeForce RTX 3070 GPU with 8GB of VRAM. We used Anaconda for dependency management, with core libraries including Python 3.7.10, Pytorch 1.8.1, pandas 1.2.2, and numpy 1.19.2.

3.2.3 Training and Validation - MacNet

The model was trained and evaluated using 5-fold cross validation. The data was fed in batches of 2 for 15 epochs. All images were standardized and rotated randomly 90,180, or 270 degrees before usage to mitigate batch effects and enhance the effective number of images. The dataset was also balanced prior to usage to ensure training data is identically distributed. For optimization, adaptive moment estimation (Adam) was used, with a learning rate of 0.0001 and weight decay of 0.0001. For our loss function, we use cross-entropy loss as this problem is a multi-class classification.

3.2.4 CellProfiler

The input 96x96 raw autofluorescent image was normalized then Sobel filtered to enhance the edges. We also used thresholding to obtain a rough estimate for the illuminated area of the cell. The normalized image and edge-enhanced image were both used to measure granularity and texture. The granularity was measured around 5px magnitude, while the texture was measured at scales of 3, 6, 9, and 16px. These measurements yield a total of 442 features for 6329 images.

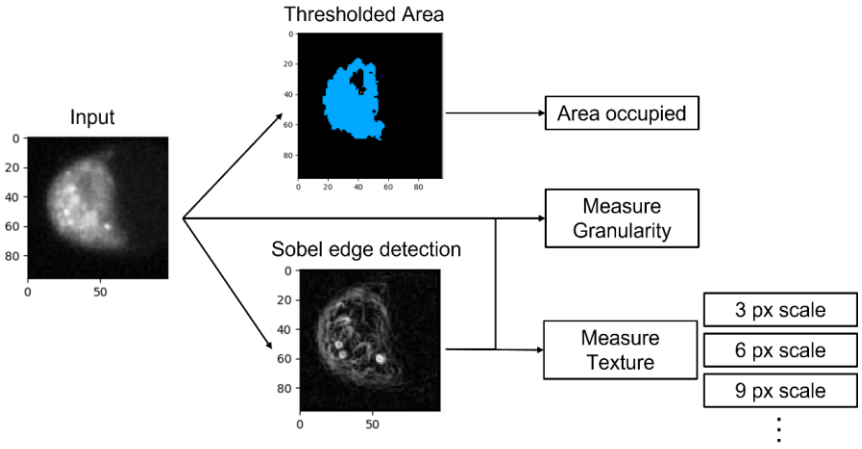

Figure 7. CellProfiler workflow. The input is thresholded to measure illuminated area. It is also processed using sobel edge detection to highlight features such as lipid droplets. Both the raw input and sobel processed image is fed into granularity and texture feature extraction modules

3.2.4.1 Conventional Models with CellProfiler Features

The features extracted using Cellprofiler were classified using a random forest classifier with 100 estimators and a K-Nearest-Neighbors (KNN) classifier with 30 neighbors.

The final KNN was trained using the raw output of Cellprofiler. Initially, a KNN was trained using decomposed primary components (PCA) extracted from the raw data, as dimension reduction is sometimes helpful to combat overfitting. The PCA-based KNN showed strictly inferior performance during testing and training and was discarded.

The random forest classifier is an ensemble of decision trees trained using random raw features as branching points. The tree separates the data at these points based on a certain feature's value until the datapoints of each branch is purely within a single class. We use 100 decision trees for our classifier.

3.3 Results for TR Macrophages/MD Macrophages/Monocyte Phenotypes

3.3.1 Classification Results for MacNet

MacNet performed very well on 5-fold cross validation for the categorization of macrophage origin. It achieved an aggregate mean test accuracy of 97.72% when classifying images from the reserved test set of TR macrophages, MD macrophages, and monocytes. This is a very high accuracy, and normally indicates the network is overfit to some degree. Nevertheless, these results show that using origin to phenotype macrophages can yield much superior results than using macrophage polarization.

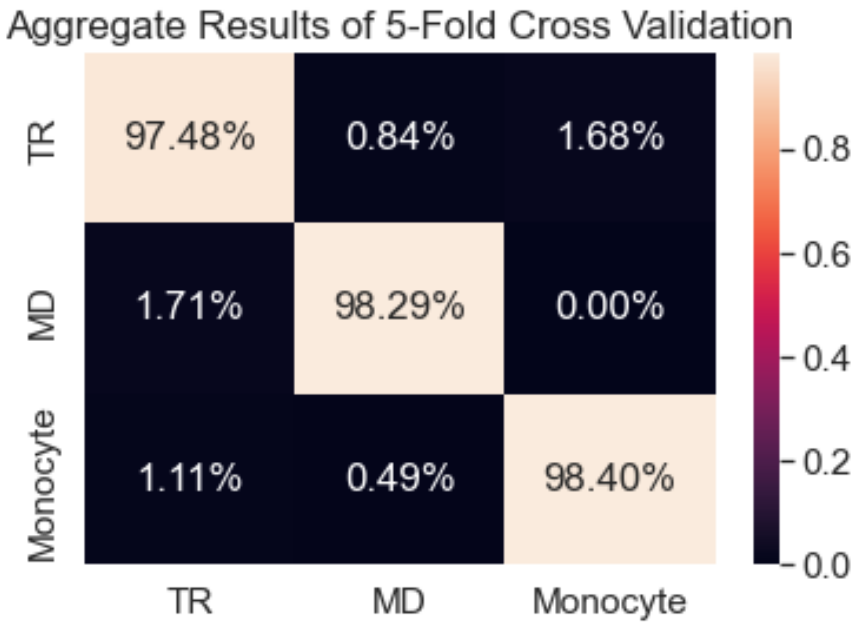

Figure 8. Aggregated confusion matrix for 5-fold cross validation of MacNet macrophage origin classification

We did not attempt to train other models for comparison in this case due to the high performance of MacNet. Larger nets like Inception V4 or PNASNet-5 would perform marginally better given more training time and samples but would likely excessively overfit on our current dataset.

Below, we show the T-SNE plot generated from the final layer of MacNet. although we see some elongated shapes in the T-SNE, the groups are also very well separated. This suggests the origin phenotypes are unique and can be classified into discrete classes. A certain degree of photobleaching is expected in long imaging sessions, which may have caused the elongated clusters.

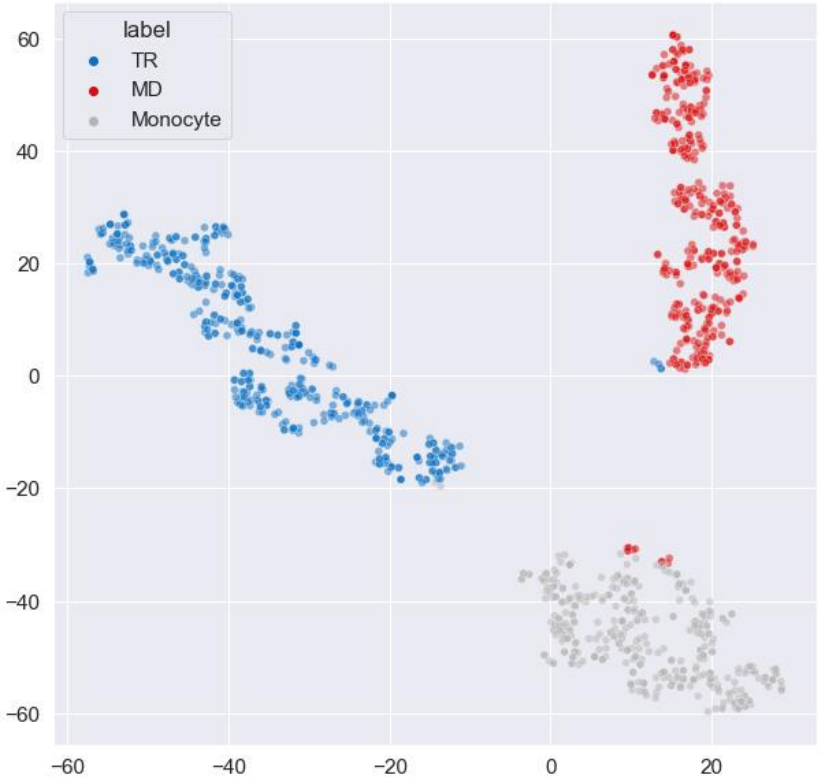

Figure 9. T-SNE of macrophage origins. The elongated clusters could suggest some temporal effects such as photobleaching or cell stress.

For the saliency map below when using MacNet to classify based on origin, we see that most activated pixels are again within the cell. The last cell on the right does display some overfitting, but still has the majority of activated pixels focused on morphological features within the cell.

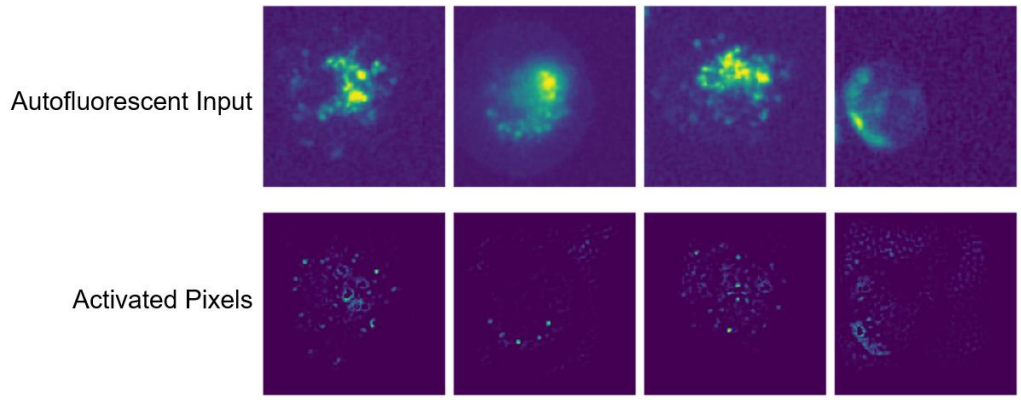

Figure 10. Saliency map of Macnet. Above is the raw autofluorescent image while below are the pixels activated to produce classification. The right-most image displays signs of overfitting as some activated pixels are outside the cell.

3.3.2 Classification Results for CellProfiler Methods

We compare CellProfiler feature engineered machine learning architectures with our deep learning model. The performances of all 3 methods are quite similar, but MacNet took around 30 minutes to train, while CellProfiler took 330 minutes to extract features from the same test set.

Table 1. Results for CellProfiler extracted images compared to MacNet

Architecture	Dataset	Accuracy
Random Forest	CellProfiler Features	99.05%
K Nearest Neighbors	CellProfiler Features	98.63%
MacNet (CNN)	Image (Normalized)	98.70%

We also measured the distribution of the most important features by extracting them from a decision tree. Some features are extracted from the raw image while others are extracted off the edges detected by a Sobel filter. The importance refers to the particular feature's weight in the extracted decision tree. From the results, we can see that both the raw input and Sobel-filtered edges provided good features, and that most of the useful features were concentrated in the 3-6 px scale.

Table 2. List of most important extracted features.

Most Important Features (Texture)	Input	Scale (px)	Importance
InfoMeasure 1	Input	6	43.49%
Difference Entropy	Edged	3	43.01%
Angular Second Moment	Edged	3	2.54%
Sum Average	Input	3	1.79%

The density plots below show that the most important measurements are not necessarily distinguishing between all phenotypes but may just be effective in separating two. Infomeasure 1 separates TRs from MDs while angular second moment of texture provides clear distinction of MDs and monocytes.

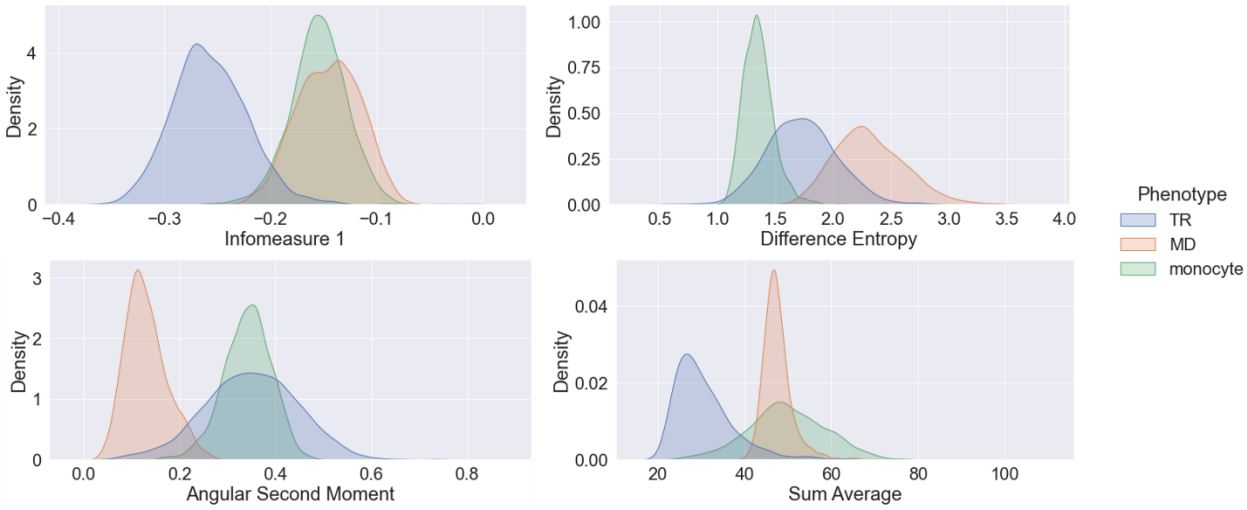

Figure 11. Distribution of measurements for some key features. All important features extracted were from the texture measurement module of CellProfiler.

T-SNE clustering was performed on the features from CellProfiler. These clusters seem much less elongated compared to the T-SNE of macnet. As these features are ultimately from the same dataset, this implies our feature extraction methods in CellProfiler normalize for adverse/changing imaging conditions. We also confirm that our feature extraction methods preserve information most relevant for categorization due to the tight and homogenous clusters.

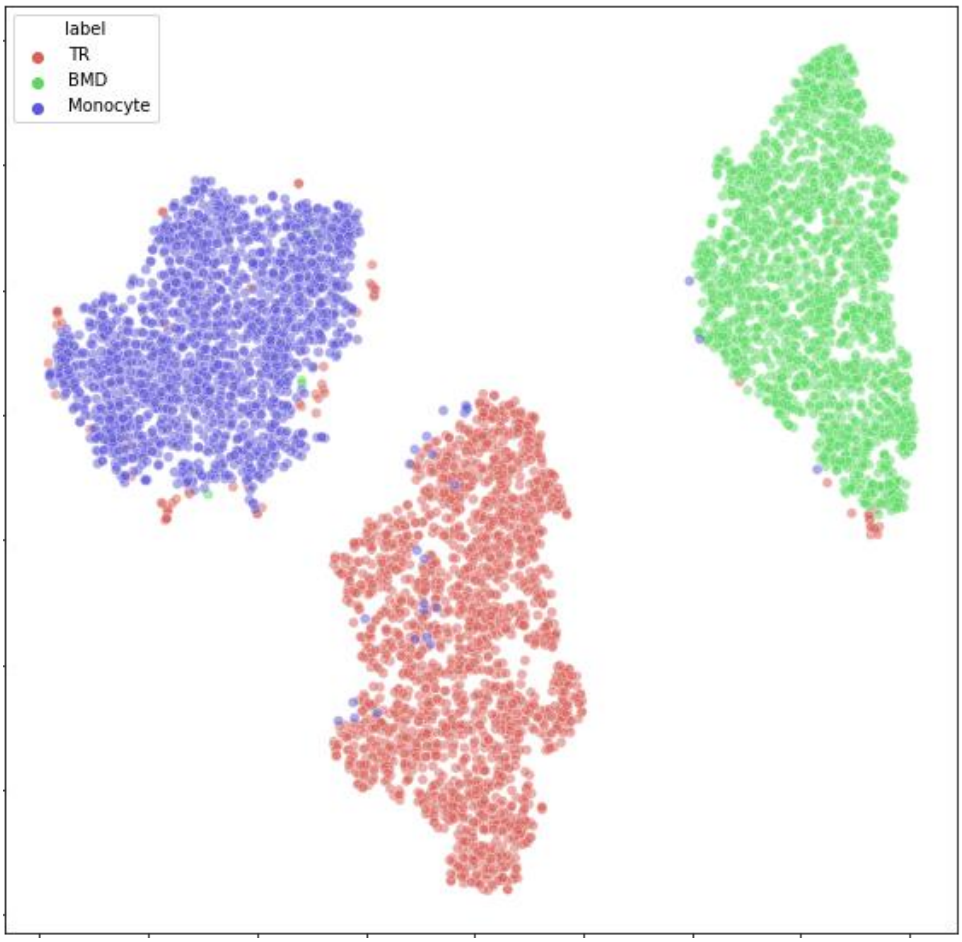

Figure 12. T-SNE of features extracted using CellProfiler. The clusters are well-separated and tightly grouped, which indicates the underlying data has distinct groups.

3.4 Discussion

Compared to phenotyping macrophages via polarization, phenotyping via origin yielded far superior results. The delta in performance can be explained by both the purer cohorts, as well as our change in imaging methodology from immunostaining to autofluorescence. Staining for mitochondria correlates with the metabolic state of the cell, which can also be examined using the autofluorescence from the metabolic enzyme NAD(P)H. Using autofluorescence also reduces stress on the cell from the immunostaining process and seems more robust to photobleaching.

MacNet and CellProfiler feature engineering performed similarly, but there are signs that CellProfiler is more robust. We can see from the T-SNEs of both approaches that CellProfiler features cluster more neatly and compactly compared to the elongated clusters of MacNet. Elongated clusters are usually due to a temporal influence on samples, which in this case could either be photobleaching or strain on the cells from being in an imaging plate for too long. It seems that the features extracted using CellProfiler may have normalized for these effects.

One advantage of the CellProfiler feature engineering is our clear understanding of what it actually measures. Texture data from the 3–6-pixel range can be used to effectively discriminate between phenotypes, as opposed to MacNet, which is a black box. We can compare these distributions to cells from different specimen and have a clearer path to generalizing the model to be specimen-agnostic.

Chapter 4: Conclusion

In this thesis we presented results for phenotyping macrophages via function and origin. We achieved a 3-way classification accuracy of 80.50% using PNASNet-5 on M0, M1, and M2 macrophage phenotypes. We found that phenotyping macrophage polarization to a higher accuracy was difficult due to incomplete differentiation of naïve macrophages into M1 and M2 activation states. We also found the different polarizations to be gradients that smoothly transitioned from phenotype to phenotype, rather than discrete classes. Conversely, phenotyping via origin was much more successful. We achieved classification accuracies of 98.70% using MacNet and 99.05% using random forest with CellProfiler features extracted from the raw image.

While the results for phenotyping via macrophage origin are promising, there were some parts of the experiment that could be improved. Instead of using cells from one specimen, we should incorporate multiple specimens to ensure we are finding general features rather than specimen specific features. We can also optimize imaging method to reduce background in the image, which may help with overfitting on the background instead of cell morphology. It may be better to image smaller batches of cells at a time to reduce stress on the cells. Although photobleaching was minimal, we should image autofluorescence on a single channel, as all channels were approximately the same.

For future work, we plan to generalize our model to different murine specimen, then attempt to apply it to humans. If our generalized model performs adequately, we can start comparing macrophage phenotype-based diagnosis for different disease to classical diagnosis methods.

Phenotyping macrophages have the potential to become another powerful tool for the research and diagnosis of a plethora of diseases. In this thesis we have shown that although macrophage phenotypes are still not a well-defined field, we can use both deep learning and feature engineering to effectively phenotype macrophages.

Bibliography

[1] T. C. Moreira Lopes, D. M. Mosser, and R. Gonçalves, “Macrophage polarization in intestinal inflammation and gut homeostasis,” *Inflamm. Res.*, vol. 69, no. 12, pp. 1163–1172, Dec. 2020, doi: 10.1007/s00011-020-01398-y.

[2] H. M. Rostam, P. M. Reynolds, M. R. Alexander, N. Gadegaard, and A. Ghaemmaghami, “Image based Machine Learning for identification of M1 and M2 macrophages,” 2016, doi: 10.13140/RG.2.2.27714.48328.

[3] Y. Zhu *et al.*, “Tissue-Resident Macrophages in Pancreatic Ductal Adenocarcinoma Originate from Embryonic Hematopoiesis and Promote Tumor Progression,” *Immunity*, vol. 47, no. 2, pp. 323-338.e6, Aug. 2017, doi: 10.1016/j.immuni.2017.07.014.

[4] S. Xu and M. L. Shinohara, “Tissue-Resident Macrophages in Fungal Infections,” *Front. Immunol.*, vol. 8, p. 1798, 2017, doi: 10.3389/fimmu.2017.01798.

[5] S. Bhatia *et al.*, “Rapid Host Defense against Aspergillus fumigatus Involves Alveolar Macrophages with a Predominance of Alternatively Activated Phenotype,” *PLoS ONE*, vol. 6, no. 1, p. e15943, Jan. 2011, doi: 10.1371/journal.pone.0015943.

[6] K. A. Jablonski *et al.*, “Novel Markers to Delineate Murine M1 and M2 Macrophages,” *PLOS ONE*, vol. 10, no. 12, p. e0145342, Dec. 2015, doi: 10.1371/journal.pone.0145342.

[7] S. P. Nobs and M. Kopf, “Tissue-resident macrophages: guardians of organ homeostasis,” *Trends Immunol.*, May 2021, doi: 10.1016/j.it.2021.04.007.

[8] M. M. Ahamada, Y. Jia, and X. Wu, “Macrophage Polarization and Plasticity in Systemic Lupus Erythematosus,” *Front. Immunol.*, vol. 12, p. 734008, Jan. 2021, doi: 10.3389/fimmu.2021.734008.

[9] D. G. Russell, P.-J. Cardona, M.-J. Kim, S. Allain, and F. Altare, “Foamy macrophages and the progression of the human TB granuloma,” *Nat. Immunol.*, vol. 10, no. 9, pp. 943–948, Sep. 2009, doi: 10.1038/ni.1781.

[10] S. Gordon and A. Plüddemann, “The Mononuclear Phagocytic System. Generation of Diversity,” *Front. Immunol.*, vol. 10, p. 1893, 2019, doi: 10.3389/fimmu.2019.01893.

[11] L. van de Laar *et al.*, “Yolk Sac Macrophages, Fetal Liver, and Adult Monocytes Can Colonize an Empty Niche and Develop into Functional Tissue-Resident Macrophages,” *Immunity*, vol. 44, no. 4, pp. 755–768, Apr. 2016, doi: 10.1016/j.immuni.2016.02.017.

[12] F. Ginhoux and M. Guilliams, “Tissue-Resident Macrophage Ontogeny and Homeostasis,” *Immunity*, vol. 44, no. 3, pp. 439–449, Mar. 2016, doi: 10.1016/j.immuni.2016.02.024.

[13] Q. Lahmar, J. Keirsse, D. Laoui, K. Movahedi, E. Van Overmeire, and J. A. Van Ginderachter, “Tissue-resident versus monocyte-derived macrophages in the tumor microenvironment,” *Biochim. Biophys. Acta BBA - Rev. Cancer*, vol. 1865, no. 1, pp. 23–34, Jan. 2016, doi: 10.1016/j.bbcan.2015.06.009.

[14] H. Aegerter *et al.*, “Influenza-induced monocyte-derived alveolar macrophages confer prolonged antibacterial protection,” *Nat. Immunol.*, vol. 21, no. 2, pp. 145–157, Feb. 2020, doi: 10.1038/s41590-019-0568-x.

[15] Y. Zhao, W. Zou, J. Du, and Y. Zhao, “The origins and homeostasis of monocytes and tissue-resident macrophages in physiological situation,” *J. Cell. Physiol.*, vol. 233, no. 10, pp. 6425–6439, 2018, doi: https://doi.org/10.1002/jcp.26461.

[16] K. Yamasaki and S. F. van Eeden, “Lung Macrophage Phenotypes and Functional Responses: Role in the Pathogenesis of COPD,” *Int. J. Mol. Sci.*, vol. 19, no. 2, Art. no. 2, Feb. 2018, doi: 10.3390/ijms19020582.
[17] S. M. Lai *et al.*, “Organ-Specific Fate, Recruitment, and Refilling Dynamics of Tissue-Resident Macrophages during Blood-Stage Malaria,” *Cell Rep.*, vol. 25, no. 11, pp. 3099-3109.e3, Dec. 2018, doi: 10.1016/j.celrep.2018.11.059.
[18] P.-L. Loyher *et al.*, “Macrophages of distinct origins contribute to tumor development in the lung,” *J. Exp. Med.*, vol. 215, no. 10, pp. 2536–2553, Sep. 2018, doi: 10.1084/jem.20180534.
[19] H. Liu, H. Dong, L. Jiang, Z. Li, and X. Ma, “Bleomycin inhibits proliferation and induces apoptosis in TPC-1 cells through reversing M2-macrophages polarization,” *Oncol. Lett.*, vol. 16, no. 3, pp. 3858–3866, Sep. 2018, doi: 10.3892/ol.2018.9103.
[20] J. Trial, K. A. Cieslik, S. B. Haudek, C. Duerrschmid, and M. L. Entman, “Th1/M1 Conversion to Th2/M2 Responses in Models of Inflammation Lacking Cell Death Stimulates Maturation of Monocyte Precursors to Fibroblasts,” *Front. Immunol.*, vol. 4, Sep. 2013, doi: 10.3389/fimmu.2013.00287.
[21] D. Hashimoto *et al.*, “Tissue-Resident Macrophages Self-Maintain Locally throughout Adult Life with Minimal Contribution from Circulating Monocytes,” *Immunity*, vol. 38, no. 4, pp. 792–804, Apr. 2013, doi: 10.1016/j.immuni.2013.04.004.
[22] “Fluorescence imaging - Latest research and news | Nature.” https://www.nature.com/subjects/fluorescence-imaging (accessed May 17, 2022).
[23] R. A. Hoebe, C. H. Van Oven, T. W. J. Gadella, P. B. Dhonukshe, C. J. F. Van Noorden, and E. M. M. Manders, “Controlled light-exposure microscopy reduces photobleaching and phototoxicity in fluorescence live-cell imaging,” *Nat. Biotechnol.*, vol. 25, no. 2, pp. 249–253, Feb. 2007, doi: 10.1038/nbt1278.
[24] A. Diaspro, G. Chirico, C. Usai, P. Ramoino, and J. Dobrucki, “Photobleaching,” in *Handbook Of Biological Confocal Microscopy*, J. B. Pawley, Ed. Boston, MA: Springer US, 2006, pp. 690–702. doi: 10.1007/978-0-387-45524-2_39.
[25] P. M. Schaefer, S. Kalinina, A. Rueck, C. A. F. von Arnim, and B. von Einem, “NADH Autofluorescence—A Marker on its Way to Boost Bioenergetic Research,” *Cytometry A*, vol. 95, no. 1, pp. 34–46, 2019, doi: 10.1002/cyto.a.23597.
[26] A. J. Walsh *et al.*, “Classification of T-cell activation via autofluorescence lifetime imaging,” *Nat. Biomed. Eng.*, vol. 5, no. 1, pp. 77–88, Jan. 2021, doi: 10.1038/s41551-020-0592-z.
[27] Z. Wang, D. Guan, S. Wang, L. Y. A. Chai, S. Xu, and K.-P. Lam, “Glycolysis and Oxidative Phosphorylation Play Critical Roles in Natural Killer Cell Receptor-Mediated Natural Killer Cell Functions,” *Front. Immunol.*, vol. 11, 2020, Accessed: May 19, 2022. [Online]. Available: https://www.frontiersin.org/article/10.3389/fimmu.2020.00202
[28] E. Ramond, A. Jamet, M. Coureuil, and A. Charbit, “Pivotal Role of Mitochondria in Macrophage Response to Bacterial Pathogens,” *Front. Immunol.*, vol. 10, 2019, Accessed: May 18, 2022. [Online]. Available: https://www.frontiersin.org/article/10.3389/fimmu.2019.02461
[29] Y. Li, Y. He, K. Miao, Y. Zheng, C. Deng, and T.-M. Liu, “Imaging of macrophage mitochondria dynamics in vivo reveals cellular activation phenotype for diagnosis,” *Theranostics*, vol. 10, no. 7, pp. 2897–2917, Feb. 2020, doi: 10.7150/thno.40495.

[30] M. A. Aon, N. Bhatt, and S. C. Cortassa, “Mitochondrial and cellular mechanisms for managing lipid excess,” *Front. Physiol.*, vol. 5, p. 282, Jul. 2014, doi: 10.3389/fphys.2014.00282.
[31] N. Pavillon, A. J. Hobro, S. Akira, and N. I. Smith, “Noninvasive detection of macrophage activation with single-cell resolution through machine learning,” *Proc. Natl. Acad. Sci.*, vol. 115, no. 12, pp. E2676–E2685, Mar. 2018, doi: 10.1073/pnas.1711872115.
[32] T. Toth *et al.*, “Environmental properties of cells improve machine learning-based phenotype recognition accuracy,” *Sci. Rep.*, vol. 8, no. 1, Art. no. 1, Jul. 2018, doi: 10.1038/s41598-018-28482-y.
[33] S. Berryman, K. Matthews, J. H. Lee, S. P. Duffy, and H. Ma, “Image-based phenotyping of disaggregated cells using deep learning,” *Commun. Biol.*, vol. 3, no. 1, pp. 1–9, Nov. 2020, doi: 10.1038/s42003-020-01399-x.
[34] C. Ounkomol, S. Seshamani, M. M. Maleckar, F. Collman, and G. R. Johnson, “Label-free prediction of three-dimensional fluorescence images from transmitted-light microscopy,” *Nat. Methods*, vol. 15, no. 11, Art. no. 11, Nov. 2018, doi: 10.1038/s41592-018-0111-2.
[35] Z. Wang, Y. Xie, and S. Ji, “Global voxel transformer networks for augmented microscopy,” *Nat. Mach. Intell.*, vol. 3, no. 2, Art. no. 2, Feb. 2021, doi: 10.1038/s42256-020-00283-x.
[36] M. Tan and Q. V. Le, “EfficientNet: Rethinking Model Scaling for Convolutional Neural Networks,” *ArXiv190511946 Cs Stat*, Sep. 2020, Accessed: Apr. 08, 2022. [Online]. Available: http://arxiv.org/abs/1905.11946
[37] C. Szegedy, S. Ioffe, V. Vanhoucke, and A. Alemi, “Inception-v4, Inception-ResNet and the Impact of Residual Connections on Learning,” *ArXiv160207261 Cs*, Aug. 2016, Accessed: Apr. 08, 2022. [Online]. Available: http://arxiv.org/abs/1602.07261
[38] C. Liu *et al.*, “Progressive Neural Architecture Search,” *ArXiv171200559 Cs Stat*, Jul. 2018, Accessed: Apr. 08, 2022. [Online]. Available: http://arxiv.org/abs/1712.00559
[39] S. Xie, R. Girshick, P. Dollár, Z. Tu, and K. He, “Aggregated Residual Transformations for Deep Neural Networks,” *ArXiv161105431 Cs*, Apr. 2017, Accessed: Apr. 08, 2022. [Online]. Available: http://arxiv.org/abs/1611.05431
[40] R. Wightman, *PyTorch Image Models*. 2022. Accessed: Apr. 12, 2022. [Online]. Available: https://github.com/rwightman/pytorch-image-models